Cavity Ionization as a Function of Wall Material

Frank H. Attix,[1] LeRoy DeLa Vergne, and Victor H. Ritz

A study has been made of the ionization within a flat cavity chamber under irradiation by X- and gamma rays in the energy region 38 to 1,250 kilovolts effective (kev).   Chamber walls were made of carbon, aluminum, copper, tin, and lead, and the wall separation was varied from 0.5 to 10 millimeters.   Results are compared with cavity theory.

1. Introduction

In 1953 an experimental study of cavity ionization [2] was carried out at the Bureau by means of a chamber of the parallel-plate type, having walls of C, Al, Cu, Sn, or Pb, which could be varied in separation from about 0.5 to 10 mm. The gas between the plates was air at room temperature and temperature. Relative ionizations were compared when the chamber was irradiated by heavily filtered X-rays of 50 to 250 kv, and by γ-rays from Au [198] (411 kev), Cs [137] (670 kev), and Co [60] (1,250 kev). For the X-rays, measurements of ionization were also made with a free-air chamber.

The results were presented in informal communications which were intended for limited distribution and were not, therefore, generally available. The work has not been published heretofore because, in retrospect, it was regarded as preliminary in nature and because the chamber design was not ideally suited to the problem.

The principal objections to the design of the experimental ionization chamber are that: (a) It should have side walls to eliminate the escape of electrons from between the plates; and (b) varying the gas-pressure instead of the separation of the plates would give the experiment greater accuracy and simplicity. Several experiments have since been done here and elsewhere [1 to 4] [3] employing pressure-variation in closed cavities, and there can be no doubt as to the inherent advantages of the method.

In spite of its shortcomings, however, the present experiment does yield some information about cavity ionization, particularly for small wall separations where the electron losses are negligible. Furthermore, the apparatus and results have recently been referred to in several published papers [2, 4, 5, 6, 7], indicating a general interest which makes the present publication of the work worthwhile.

Measurements with the γ-rays from Co [60] have recently been repeated to determine the degree of the electron losses at that energy, and to eliminate, by increasing the filtration of the γ-ray beam, the effect of low-energy scattered radiation originating in the source and its housing.

2. Experimental Apparatus

2.1. Ionization Chamber

Figure 1 shows a section through the chamber, indicating its design. The collecting volume was 5 cm in diameter, and the irradiated area about twice this size, providing some compensation for electron losses by irradiation of the guard-ring area. Connection with the collecting electrode was made through a fine wire embedded in the rear supporting wall. This wall was constructed of two sheets of polyethylene, bonded together (with the wire between) by heating, to give a total thickness of 1.8 mm.

Thin foils were cemented to the polyethylene and the groove cut afterward with a lathe tool. Thicker metal walls were precut into collector and guard ring, then attached to the polyethylene by means of double adhesive tape,[4] which gave a very strong bond. It
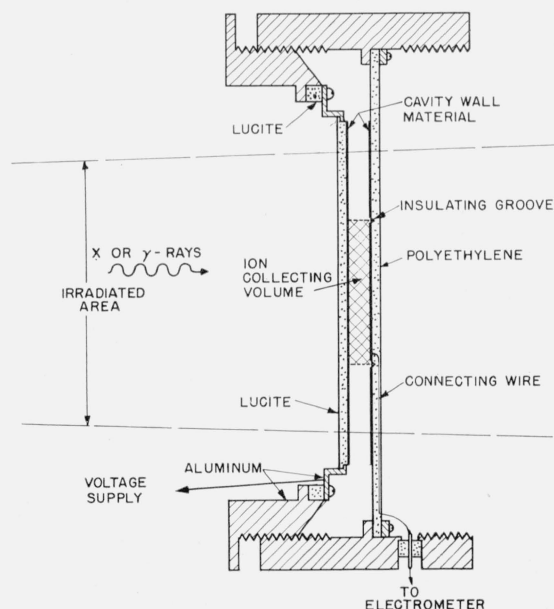

FIGURE 1. *Cross section of experimental ionization chamber.*

was found necessary to fill the 0.25-mm-wide gap between the guard ring and collecting electrode with a strip of polyethylene to avoid ion collection from that volume.

The front [5] chamber wall was supported on a screw of 1-mm pitch, to allow variation of the wall separation. The collecting voltage was applied to this wall; ±22 v/mm was found to be an adequate gradient for saturation.

The effective position of the chamber for a given separation was taken to be midway between the front and back walls.

2.2. Wall Materials

Table 1 gives the thicknesses of the walls used for the various energies. In each case the thickness is greater than that necessary for electronic equilibrium. Thicknesses of supporting materials, if present, are also shown. Attenuation and scattering from both the front and back walls were corrected for in the usual manner by varying the thicknesses (always maintaining at least equilibrium thickness) and extrapolating the observed ionization to zero wall thickness. In most cases this correction was only a few percent, but for low X-ray energies the attenuation in the front walls of high-atomic number became larger, reaching about 60 percent for the lead wall with 38-kev X-rays.

Spectroscopic analysis of the wall materials indicated that the impurities present would alter the ionization by less than 1 percent for any of the radiations used in the experiment.

---

[5] The chamber was ordinarily placed with this wall toward the source. No difference in response was observed whether the front or back of the chamber faced the source, if appropriate wall-attenuation corrections were applied.

2.3. Measurement of Ionization Current and Wall Separation

Ionization currents were measured by means of a vibrating-reed electrometer employed in a null method. Currents larger than 10^{-12} amp were passed through high megohm resistors and the IR drop balanced by a calibrated potentiometer. Smaller currents were measured by observing the rate of charge of a 10^{-11}-f calibrated capacitor.

Each current measurement was made with both polarities and averaged to eliminate the effects of: (a) Extracameral ionization; (b) radiation-induced leakage of current through the polyethylene rear supporting wall; and (c) current of energetic electrons crossing the chamber from one wall to the other. Positive and negative currents were found to agree closely except for separations less than 1 mm, where they diverged by as much as a few percent.

The plate separation was measured electrically (in the absence of radiation), employing the curcuit shown in figure 2. The two potentiometers were
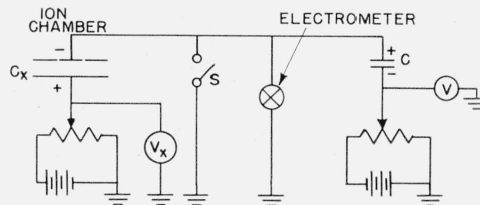

FIGURE 2. *Circuit used in determining the separation of the chamber walls by measurement of the capacitance between them.*

TABLE 1. *Thicknesses of wall materials*

Gamma or X-ray effective;[1] photon energy	Graphite		Al		Cu		Sn		Pb	
	Front wall	Rear wall	Front wall	Rear wall	Front wall	Rear wall	Front wall	Rear wall	Front wall	Rear wall
kev										
38	307 mg/cm²	307 mg/cm² +0.072 in. polyethylene.	109 mg/cm² +0.062 in. lucite.	109 mg/cm² +0.072 in. polyethylene.	23.5 mg/cm² +0.062 in. lucite.	68 mg/cm² +0.072 in. polyethylene.	10 mg/cm² +0.062 in. lucite.	57 mg/cm² +0.135 in. polyethylene.	60 mg/cm² +0.062 in. lucite.	50 mg/cm² 0.072 in. polyethylene.
70	do	do	do	do	do	do	do	do	do	Do.
118	do	do	do	do	65.5 mg/cm² +0.062 in. lucite.	do	57 mg/cm² +0.135 in. polyethylene.	do	do	Do.
169	do	do	do	do	do	do	do	do	do	Do.
206	do	do	do	do	do	do	do	do	124 mg/cm² +0.062 in. lucite.	124 mg/cm² +0.072 in. polyethylene.
411	do	do	do	do	925 mg/cm²	925 mg/cm² +0.072 in.	770 mg/cm²	770 mg/cm² +0.072 in. polyethylene.	872 mg/cm² +0.062 in. lucite.	872 mg/cm² +0.072 in. polyethylene.
670	do	do	do	do	do	do	do	do	do	Do.
1,250	do	do	437 mg/cm²	437 mg/cm² +0.072 in. polyethylene.	do	do	do	do	do	Do.

[1] Determined by attenuation in copper.

236

varied to balance a charge on C by an equal charge on C_x (the chamber capacitance), the balance being indicated by the vibrating-reed electrometer. This procedure was repeated at each of several settings of the chamber screw, using the same setting of potential V each time (i. e., constant charge). If V_x is plotted versus the indicated settings of the screw, a linear relationship results, intersecting the $V_x=0$ axis at the screw setting where the wall separation is zero. This can be shown as follows:

$$q = \text{constant} = VC = V_x C_x$$

and

$$C_x = \frac{KA}{d}$$

where:

V = voltage on known capacitor,
C = capacitance of known capacitor,
V_x = voltage applied to chamber wall,
C_x = capacitance between walls of chamber,
K = constant,
A = effective area of collecting electrode, and
d = wall separation.

Combining the two equations, we have

$$d = \left[\frac{KA}{q}\right] V_x$$

where the bracket term is the slope of the observed plot of V_x versus screw setting. Thus the separation is obtained for any measured value of V_x by multiplying it by the previously determined slope, which need be measured only once for each rear-wall assembly.

Note that the actual value of C is not needed in finding the separation. However, if it is known, one can solve for A and thence the diameter of the collecting electrode. This was found to agree with the directly measured diameters to within 1 percent.

3. X-ray Measurements

3.1. Source of X-rays

A Westinghouse 250-kv tube was operated with a well-stabilized constant potential generator to provide the X-ray source. The beam was collimated to give a diameter about twice that of the collector at 1-m distance, where the chamber was located. The kilovoltages and filtrations used are given in table 2, and are similar to those of Ehrlich and Fitch [8].[6] The effective energies were obtained from attenuation data in copper, referring to the attenuation coefficients of White [9]. These X-ray spectra are, of course, not monochromatic, but consist of a spread of photon energies [8]. Further narrowing of the spectra by increased filtration would have made the beam intensities too low for accurate measurements.

[6] Note that the filtration data given for 150 kv in this reference are in error, according to private communication with the authors.

Constant potential applied to X-ray tube	Added filtration [1]	Effective X-ray energy [2]
kev	*mm*	
50	0.125 Pb	38
100	.52 Pb	70
150	1.53 Sn+4.00 Cu	118
200	0.70 Pb+4.00 Sn+0.59 Cu	169
250	2.70 Pb+1.00 Sn+.59 Cu	206

[1] The inherent filtration of the X-ray tube was equivalent to 3-mm Al.
[2] As determined from attenuation measurements in copper.

Uniformity of the beam over the area of the chamber was ascertained by photographic densitometer measurements.

3.2. Free-Air Chamber

The exposure-dose rate (in roentgens per unit time) of the X-rays in the plane of the experimental chamber was measured by replacing that chamber with a free-air chamber having a defining diaphragm 8 mm in aperture diameter. The 12-cm plate separation of this chamber [10] was inadequate for the heavily filtered X-rays used, and it was, therefore, calibrated against the NBS 250-kv standard free-air chamber [11].

3.3. Results with X-rays

Figures 3 to 7 show the curves obtained for the ratio of ionization density in the experimental chamber to that in the calibrated free-air chamber, as a function of the wall separation in the former. Corrections for wall attenuation and scattering in the experimental chamber walls have been included.

The shapes of the curves are influenced by two effects: (a) The transition from wall-dependent ionization at small separations to air-dependent ionization at large separations, and (b) the loss of electrons out the edges of the chamber, an effect that becomes more pronounced at large separations and high X-ray energies. For walls of atomic number higher than air, the flux of electrons generated within the wall material will be greater than that in air because of the greater coefficient for absorbing energy from X-rays, (due to photoelectric effect), and because of the lower electron stopping-power (in cm²/electron) of the wall material. Furthermore, the increased reflection of electrons from walls of high-atomic number results in larger electron losses from the edge of the chamber. Thus one expects the ionization to rise as the wall separation is decreased in such a chamber, as indicated in figures 4 to 7. It is interesting to note the somewhat steeper descent of the 38-kev curve for Sn (fig. 6), as compared with that for Pb (fig. 7). (At this energy the edge losses are negligible because of the short ranges of the electrons present.) The K-edge for photoelectric absorption in Sn is located at 29 kev, giving a large component of photoelectrons with energies of the order of 9 kev (see table 5). The range of
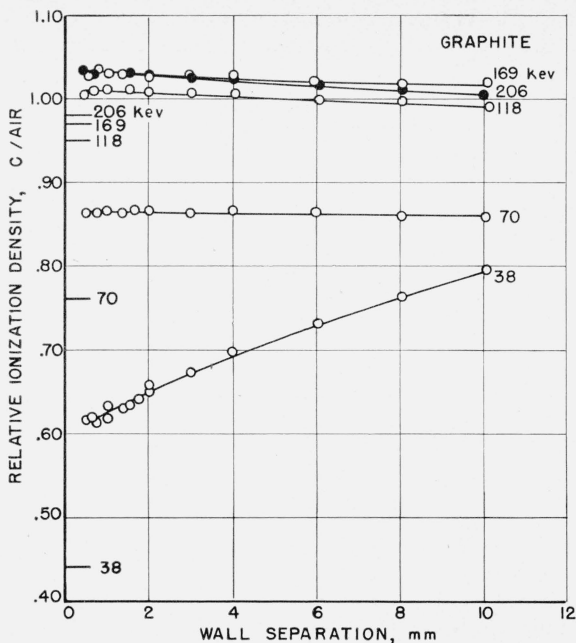
FIGURE 3. *Curves showing the ratio of ionization per unit volume in the experimental chamber to that in the free-air chamber, as a function of the separation of the walls in the experimental chamber.*

The marks at the vertical axis, labeled with the appropriate values of X-ray energy in kilovolts effective, indicate the corresponding theoretical ratios from the Bragg-Gray relation.
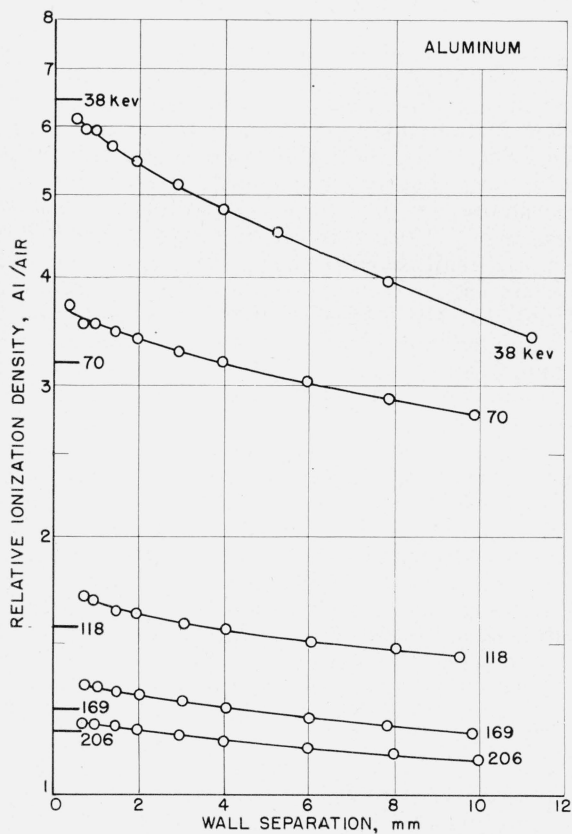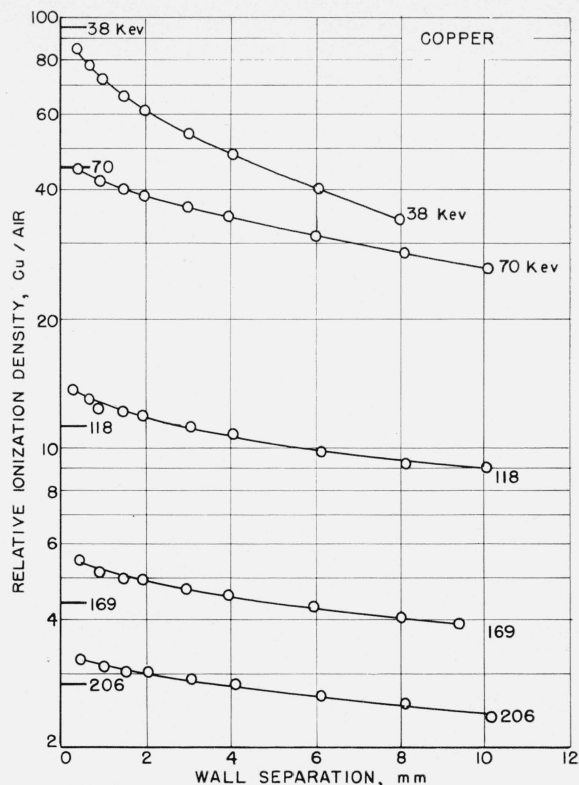

FIGURE 5.

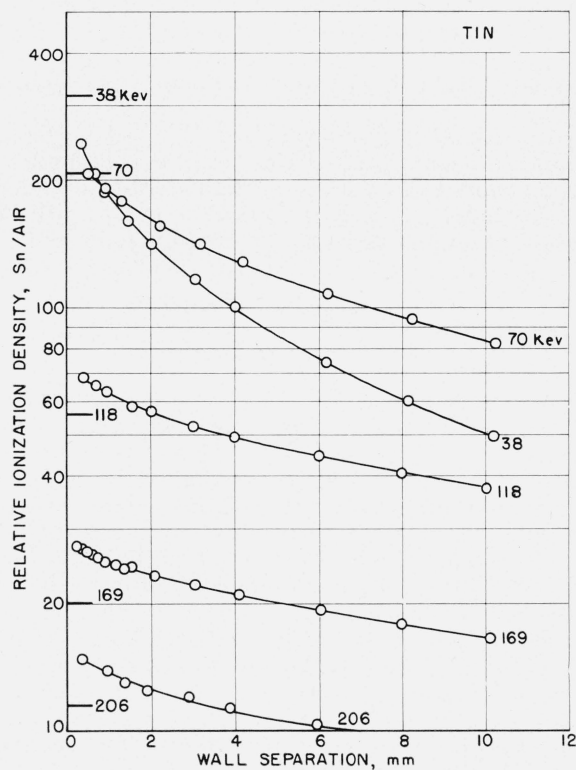(See caption for fig. 3)

FIGURE 4.

(See caption for fig. 3)

FIGURE 6.

(See caption for fig. 3)

FIGURE 7.

(See caption for fig. 3)

electrons present, and the ionization contributed by electrons generated in the gas directly by X-rays must be negligible. These requirements are difficult to fulfill with low-energy X-rays, because of the short ranges of the electrons present. Moreover, the theory itself is only an approximation, as it neglects the production (through collision) of energetic secondary electrons by the Compton-recoil electrons and photoelectrons in traversing the wall material and the air.[7]

Table 3 lists the values of the ratio $(\mu_{en})_Z/(\mu_{en})_{air}$, calculated from the X-ray attenuation coefficients of White [9], assuming the X-ray spectra to be monochromatic at the effective energy. (μ_{en}) is the sum of the photoelectric coefficient (less fluorescence losses) and the "true" Compton coefficient σ_a.[8]

TABLE 3. *Ratios of energy-absorption coefficients μ_{en} (in $cm^2/$ electron) relative to air*

Effective photon energy	$(\mu_{en})_Z/(\mu_{en})_{air}$				
	C	Al	Cu	Sn	Pb
Kev					
38	0.45	5.62	70.6	176	176
70	.77	2.79	34.6	136	90.2
118	.96	1.37	8.78	38.8	78.5
169	.98	1.11	3.41	14.2	38.5
206	.99	1.05	2.24	8.29	24.4
411	1.00	1.00	1.15	2.00	5.37
670	1.00	1.00	1.04	1.29	2.55
1,250	1.00	1.00	1.00	1.10	1.56

The stopping-power calculations were done by means of Bethe's formula,[9] using the mean-excitation potentials of Bakker and Segre [16] as modified for the binding correction by Bethe and Ashkin [15]. The values used were $I_{air}=80.5$ ev, $I_C=76.4$ ev, $I_{Al}=150$ ev, $I_{Cu}=276$ ev, $I_{Sn}=463$ ev, and $I_{Pb}=705$ ev. The correction for density effect according to Sternheimer [17] was included.

The stopping-power ratio of air to wall material $(1/s)$, evaluated over the electron spectrum present, is obtained [6] from the integration

$$\frac{1}{s}=\frac{1}{T_0}\int_0^{T_0}\frac{S_{air}}{S_{wall}}dT$$

where T_0 is the intial energy of the electrons generated in the wall material by X- or γ-rays, and s is the stopping power (per electron/cm^2) of the air or wall for an electron of energy T. Values of $(1/s)$ are tabulated as a function of T_0 in table 4.
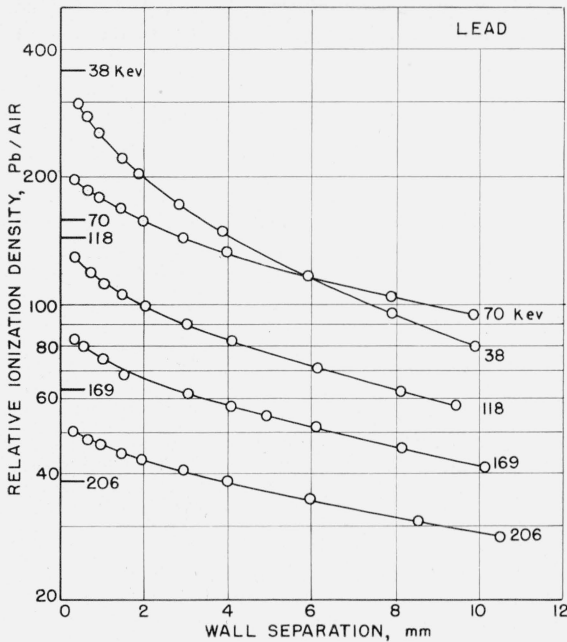
such electrons in air is about 2 mm. On the other hand, in lead the K-orbit electrons do not interact with 38-kev X-rays, and the L-shell photoelectrons predominate. These have energies in the vicinity of 22 kev, and ranges of about 1 cm. Thus this curve is less steep than the corresponding one for Sn. Similar arguments can be applied to explain the trends of the other curves at 38 and 70 kev, referring to table 5 for dominant electron energies. At higher X-ray energies the edge losses of electrons begin to predominate. Here the slopes are not strongly dependent on X-ray energy, because the electron ranges are large compared with the lateral chamber dimensions.

3.4 Comparison with Cavity Theory

The Bragg-Gray theory of cavity ionization [12,-13,6] gives for the ratio of ionizations per gram of air in two cavity chambers, A and B:

$$\frac{J_A}{J_B}=\frac{(\mu_{en})_A}{(\mu_{en})_B}\frac{s_B}{s_A}$$

where s is the ratio of electronic stopping powers (per electron/cm^2) of the wall material to air, evaluated for the electron spectrum present. If cavity B is a free-air chamber, $s_B=1$ and the above formula is further simplified.

μ_{en} is defined as the sum of those fractions of the photoelectric-, Compton-, and pair-production attenuation coefficients for γ-rays, representing energy converted from electromagnetic energy into electron-kinetic energy. The units of μ_{en} are cm^2/electron throughout this paper [14].

For valid application of this theory, the cavity must be small in comparison with the ranges of the

[7] A recently proposed modification to the theory [6] takes the "knock-on" secondary electrons into account and relates ionization to cavity size. This has not been applied here to the X-ray results because the necessary electron spectra have not been calculated for low-electron starting energies. This modified theory is, however, compared with the results of the γ-ray measurements, for which the calculated electron spectra are available.

[8] A small fraction of μ_{en} for Pb and Sn at 1,250 kev is attributable to pair production, see table 5.

[9] See eq (52), p. 254 in reference [15].

TABLE 4. *Stopping power ratio, (1/s),[1] air to wall material*

Initial electron energy T_0	1/s				
	C	Al	Cu	Sn	Pb
Mev					
0.001	0.981	1.304	1.856	2.90	5.33
.003	.983	1.258	1.691	2.42	3.88
.007	.986	1.209	1.531	2.01	2.84
.01	.987	1.191	1.476	1.882	2.54
.03	.989	1.148	1.348	1.600	1.939
.07	.991	1.124	1.283	1.468	1.690
.1	.991	1.116	1.262	1.427	1.617
.3	.993	1.096	1.213	1.335	1.463
.7	.999	1.085	1.189	1.286	1.386
1.0	1.004	1.081	1.182	1.270	1.360
1.4	1.011	1.079	1.179	1.257	1.339
2.0	1.020	1.080	1.178	1.246	1.320

$$[1] \quad (1/s) = \frac{1}{T_0} \int_0^{T_0} \frac{S_{air}}{S_{wall}} \, dT.$$

The Compton process, of course, produces a continuous spread of initial electron energies T_0. For present purposes, this distribution was approximated by a monoenergetic-starting energy given by $(\sigma_a/\sigma)h\bar{\nu}$ where σ_a is the Compton "true" absorption coefficient, σ is the total Compton coefficient, and $h\bar{\nu}$ is the γ-ray energy or the effective energy of the X-ray spectrum. Photoelectrons are taken to have initial energy equal to that of the incident photon less the binding energy of the electron in its orbit. Table 5 lists the values of T_0 which apply to air and the wall materials studied, together with the relative importance of each energy-absorbing process present in the materials.

Mean values $(\overline{1/s})$, of the stopping-power ratios $(1/s)$, evaluated for the γ-ray and effective X-ray energies, are given in table 6. These data were obtained from tables 4 and 5 as described in the footnote following table 6.

The theoretical ionization ratios J_Z/J_{air} are then obtained by taking the product of corresponding terms in tables 3 and 6. The resulting values are plotted as short lines at the y-axes in figures 3 to 7 for X-rays.

It will be seen that, while the agreement between theory and experiment at small separations is not particularly close, neither is it unsatisfactory in view of the approximations used in applying the theory, and the approximate nature of the theory itself.

In the case of the graphite wall, it is particularly difficult to satisfy the requirement that the cavity be small enough to make negligible the ionization produced by electrons originating in the air itself. This is because, as can be seen from table 5, the air has considerably more photoelectric effect than does the graphite for X-rays below 100 kev. This may account for the large discrepancies between theory and experiment in figure 3 at 38 and 70 kev.

At 169 and 206 kev, the graphite chamber apparently reads higher than the free-air chamber by about 4 percent. Probably the major factor con-

TABLE 5. *Initial electron-energy distribution*

Effective photon energy	Type of electron	Air		C		Al		Cu		Sn		Pb	
		1	2	1	2	1	2	1	2	1	2	1	2
38	Compton	2	0.15	2	0.33	2	0.03	2	0	2	0	2	0
	K-photo							29	0.91	9	0.66	------	0
	L-photo	38	.85	38	.67	37	.97	38	.09	38	.34	22	0.76
	M-photo											34	.24
70	Compton	7	.66	7	.85	7	.24	7	.02	7	.01	7	.01
	K-photo							61	.90	41	.82	------	0
	L-photo	70	.34	70	.15	69	.76	70	.08	70	.17	54	.79
	M-photo											66	.20
118	Compton	19	.94	19	.97	19	.68	19	.11	19	.03	19	.02
	K-photo							109	.82	89	.84	30	.66
	L-photo	118	.06	118	.03	117	.32	118	.07	118	.13	102	.27
	M-photo											114	.05
169	Compton	34	.98	34	1.00	34	.88	34	.29	34	.07	34	.03
	K-photo							160	.66	140	.81	81	.76
	L-photo	169	.02	169	0	168	.12	169	.05	169	.12	153	.18
	M-photo											165	.03
206	Compton	46	.99	46	1.00	46	.94	46	.45	46	.12	46	.04
	K-photo							197	.51	177	.77	118	.78
	L-photo	206	.01	206	0	205	.06	206	.04	206	.11	190	.15
	M-photo											202	.03
411	Compton	129	1.00	129	1.00	129	1.00	129	.87	129	.50	129	.19
	K-photo							402	.12	382	.44	323	.69
	L-photo	411	0	411	0	410	0	411	.01	411	.06	395	.10
	M-photo											407	.02
670	Compton	257	1.00	257	1.00	257	1.00	257	.96	257	.78	257	.40
	K-photo							661	.04	641	.20	582	.52
	L-photo	670	0	670	0	669	0	670	0	670	.20	654	.07
	M-photo											666	.01
1,250	Compton	588	1.00	588	1.00	588	1.00	588	1.00	588	.90	588	.65
	K-photo	------	------	------	------	------	------	------	------	1,220	.08	1,160	.30
	L-photo	------	------	------	------	------	------	------	------	1,250	.01	1,230	.04
	M-photo	------	------	------	------	------	------	------	------	1,250		1,250	.005
	Pair	------	------	------	------	------	------	------	------	114	.01	114	.005

Columns 1 _____ Average initial energy T_0 (in kev) of electrons produced by the indicated processes.
Columns 2 _____ Fraction of total flux of electron energy carried by electrons resulting from the indicated processes.

tributing to this effect is that the experimental chamber receives more scattered radiation from the X-ray beam than does the free-air chamber. The diaphragms in the latter chamber admit only the primary rays and those scattered in a nearly forward direction. This probably also contributes to the discrepancies between theory and experiment for the other wall materials in figures 4 to 7 as well.

TABLE 6. *Mean stopping-power ratios* $\overline{(1/s)}$,[1] *air relative to wall material*

Effective photon energy	$\overline{(1/s)}$				
	C	Al	Cu	Sn	Pb
kev					
38	0.99	1.14	1.35	1.80	2.03
70	.99	1.14	1.29	1.54	1.75
118	.99	1.15	1.27	1.44	1.84
169	.99	1.14	1.27	1.40	1.64
206	.99	1.13	1.27	1.39	1.58
411	.99	1.11	1.24	1.36	1.48
670	.99	1.10	1.22	1.33	1.43
1,250	1.00	1.09	1.19	1.29	1.38

[1] These data were obtained by graphical interpolation of the data given in table 4, at the electron energies (T_0) given in columns 1 of table 5. The stopping-power ratios $(1/s)$ so obtained were then weighted by the appropriate factors given in columns 2 of table 5 to obtain $\overline{(1/s)}$.

4. γ-Ray Measurements

4.1. γ-Ray Sources

Sources consisting of several curies of Au[198], Cs[137], and Co[60] were enclosed in lead housings to provide collimated beams as for the X-ray work already described. The Au[198] and Cs[137] source-housings were constructed to allow the rays going in a rearward direction to escape through a hole, thus avoiding the production of 180° backscattered γ-rays of low energy. The forward beam was filtered by 2.4-mm Sn+0.5-mm Cu+0.8-mm Al to suppress any fluorescense emitted by the lead housing.

The Co[60] source first used was a 10-curie source in a large lead housing, closed in the rearward direction and lined with brass on the inside. The first results were taken with the same filter used for the other sources, but it was found later that the scattered radiation originating in the housing and source was not adequately removed by this filter, and as a result the ionization in the chamber with high-atomic-number walls was spuriously high because of excess photoelectric effect. The final data described here were taken with a 1-curie Co[60] source 3 mm in diameter, enclosed in a lead housing relatively free of backscattering, and with a filter of 12-mm Pb in addition to the previously described filter of Sn, Cu, and Al. Additional thicknesses of lead were found not to change the observed ionization ratio of Pb/C.

The spectra of gamma rays from Au[198] and Cs[137] are nearly monochromatic, and located at 411 kev and 670 kev, respectively. Co[60] emits two lines of equal intensity at 1.17 Mev and 1.33 Mev, but for present purposes it has been assumed to be monochromatic at 1.25 Mev.

4.2. Results with γ-Rays

For the γ-ray measurements no free-air chamber was employed. Only the experimental ionization chamber was used and the relative ionization densities observed with the various wall materials. These results are given in figures 8 to 10.

As a test of the influence of the electron losses out the edge of the chamber, side walls were constructed of the various wall materials. These consisted of rings about 9 cm in diameter, thick enough for electronic equilibrium and having various depths so that
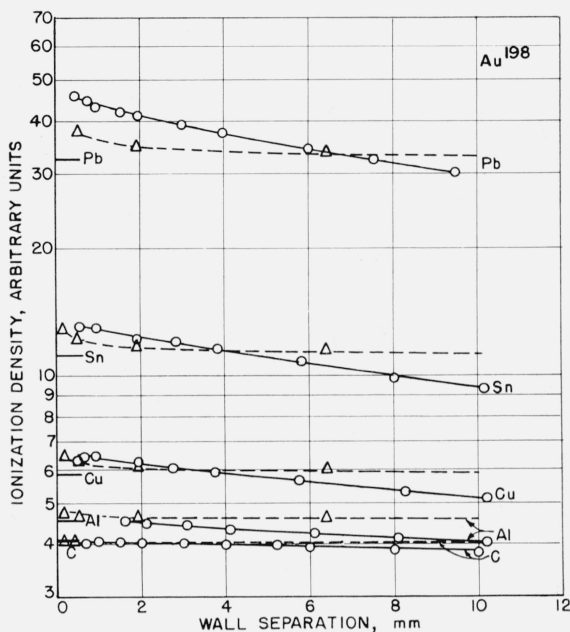
FIGURE 8. *The solid curves show the relative ionization densities measured in the experimental chamber with γ-rays from Au[198] or Cs[137].*

The marks at the vertical axis are the ionization ratios, relative to graphite, predicted by the Bragg-Gray theory. The dashed curves are the corresponding ratios predicted by the modified cavity theory. Both sets of theoretical data have been normalized to the experimental graphite curve at small separations.
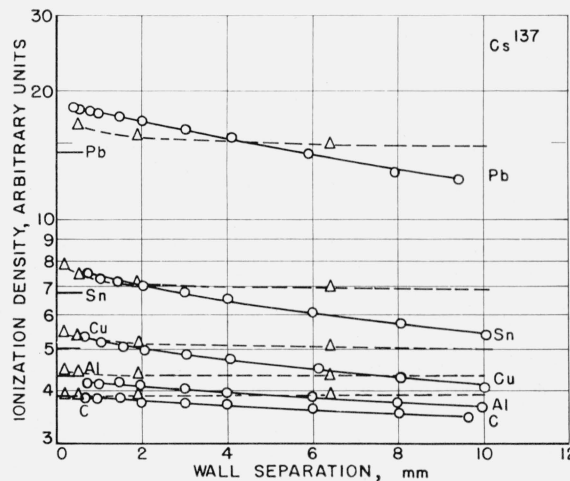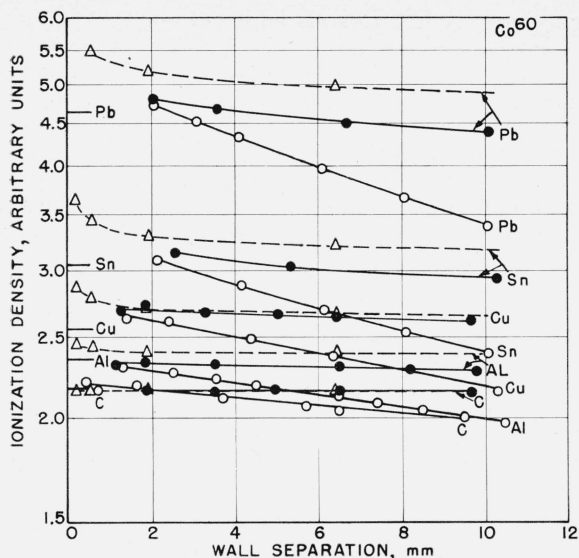
FIGURE 9.

(See caption for fig. 8)

241

FIGURES 10. *The solid curves drawn through the open circles show the relative ionization densities measured in the experimental chamber with γ-rays from Co⁶⁰, without side walls.*

The solid curves drawn through the filled circles show the corresponding results when side walls were added. The marks at the vertical axis, are the ionization ratios, relative to graphite, predicted by the Bragg-Gray theory. The dashed curves are the corresponding ratios predicted by the modified cavity theory. Both sets of theoretical data have been normalized to the experimental graphite curve (with side walls) at small separations.

the wall separation could be varied. The γ-ray beam was large enough to irradiate these rings, producing electrons to replace those lost from the collecting region. The rings were insulated both from the guard ring and the high-voltage wall of the chamber by polyethylene 0.025 mm in thickness. It was found that, for wall separations as great as 1 cm, there was a negligible difference in ionization collected whether the rings were operated at the potential of the high-voltage wall or at ground potential, indicating no field-distorting effect. Glancing angle attenuation (1) of the γ-rays striking the rings was checked by also constructing rings of 1-cm depth but with a cone shape to allow the rays to strike the inner-ring surface at a 45° angle rather than a glancing angle, resulting in much less attenuation.

Gamma-ray scattering from the rings was also measured by doubling their thickness and observing the resulting increase in ionization. Both of these effects were found to be negligible.

In figure 10 the open points indicate the ionization density observed without the edge rings, and the solid points show the results with the rings added. For the lead walls at 10-mm separation, the edge losses are seen to be about 23 percent, while for graphite they are about 9 percent. This difference is caused by the greater reflecting ability of the lead for electrons, increasing the effective solid angle for their escape out the edges. While the edge losses shown in figure 10 apply strictly to the Co⁶⁰ data only, they do give some indication of the losses at other energies where the electron ranges are long compared with the chamber dimensions. They also supply an upper limit for the magnitude of the losses at lower energies.

4.3. Comparison with Bragg-Gray Cavity Theory

Bragg-Gray theory calculations have already been described in the comparison with X-ray ionization data. Tables 3 and 6 also contain data applicable to the γ-ray results in the same fashion. However, because there are, for γ-rays, no free-air chamber results available for comparison with cavity-chamber results, the theoretical ionization ratios J_z/J_{air} have been divided by J_c/J_{air} to give J_z/J_c. These ratios are then normalized to the experimental graphite-chamber ionization density at small separations, and plotted as short lines adjacent to the y-axis in figures 7 to 10. Although they generally tend to be too low, these theoretical ratios do roughly predict the experimental-ionization ratios relative to graphite, particularly for Co⁶⁰ γ-rays.

4.4. Comparison with Modified Cavity Theory

A modified cavity theory (see footnote 7) which takes into account the production of secondary electrons and which relates the ionization to the cavity size, has also been compared with the experimental γ-ray results. The difference from the conventional Bragg-Gray treatment comes in the calculation of the stopping-power ratio $(1/s)$, the details of which are given in reference [6]. In the modified theory $(1/s)$ is a function not only of T_0, but also of a parameter Δ, which is taken to be the energy needed by an electron to cross the cavity.

In table 7 are listed the values of $\overline{(1/s)}$ obtained from this theory, based upon the same mean-excitation potentials (I) and density-effect data as were used before. Table 5 has again been used to weight $(1/s)$ by the electron-energy flux at each (mean) energy, T_0 present in a material. The approximate electron linear ranges corresponding to the values are also given, assuming the linear range to be about 0.8 times the actual electron-track length [18].

T_0 compare these data with the experimental results, one must assign an effective size to the experimental-chamber cavity. This has been taken to be simply the plate separation, because the accurate choice of Δ is not critical.

The product of the terms in table 7 with the corresponding terms in table 3 yields the theoretical ionization ratios relative to air, according to the modified theory. Having renormalized the data to be relative to graphite, as was done before for the Bragg-Gray results, they are plotted as dashed curves in figures 8 to 10.

It is interesting to note how closely the theory predicts the variation of ionization with chamber size for Co⁶⁰, where the edge losses of electrons are eliminated. The agreement between this theory and the experimental results otherwise is not very exact, although it generally seems to be an improvement upon the other theory, particularly at small separations. Recent ionization measurements by Greening [2], by Whyte [3], and by Attix and Ritz [1], also confirm that the modified cavity theory gives improved agreement and predicts closely the

Wall material	γ-ray energy	Electron range (mm air)				
		0.15	0.51	1.9	6.4	22
		Δ(kev)				
		2.5	5.1	10.2	20.4	40.9
C	*Mev* 0.411	0.99	0.99	0.99	0.99	0.99
	.670	.99	.99	.99	.99	.99
	1.25	.99	.99$_5$	1.00	1.00	1.00
Al	0.411	1.14	1.13	1.12	1.11	1.10
	.670	1.14	1.12	1.11	1.10$_5$	1.10
	1.25	1.13	1.12	1.11	1.10	1.09
Cu	0.411	1.35	1.31	1.27$_5$	1.25	1.23
	.670	1.33$_5$	1.29	1.26	1.24	1.22
	1.25	1.32	1.28	1.25	1.23	1.21
Sn	0.411	1.56$_5$	1.48	1.42	1.38	1.35
	.670	1.55	1.46	1.41	1.37	1.34
	1.25	1.52	1.44	1.38$_5$	1.35	1.32
Pb	0.411	------	1.68	1.58	1.52	1.47
	.670	------	1.65	1.56	1.50	1.45
	1.25	------	1.62	1.53	1.47	1.43

variation of ionization with cavity size. In particular, reference [1] shows very close agreement between theory and experiment with Co^{60} γ-rays and chamber walls of C, Al, and Cu. Other recent work in this laboratory [19] has also confirmed the agreement between a graphite cavity chamber and a pressurized free-air chamber in measuring exposure dose (in roentgens) of γ-rays from Co^{60} and Cs^{137}, after cavity-theory corrections are applied to the graphite chamber results.

---

5. References

[1] F. H. Attix and V. H. Ritz, A determination of the γ-ray emission of radium, J. Research NBS **59**, 293 (1957) RP2801.
[2] J. R. Greening, An experimental examination of theories of cavity ionization, Brit. J. Radiol. **30**, 254 (1957).
[3] G. N. Whyte, An attempt to measure the Bragg-Gray stopping power correction, Radiation Research (in press).
[4] H. V. Larson, Radiation Research **5**, 558 (1956).
[5] G. J. Hine and G. L. Brownell, Radiation dosimetry (Academic Press, New York, N. Y., 1956).
[6] L. V. Spencer and F. H. Attix, Radiation Research **3**, 239 (1955).
[7] J. McElhinney, B. Zendle, and S. R. Domen, Radiation Research **6**, 40 (1957).
[8] M. Ehrlich and S. H. Fitch, Nucleonics **9**, No. 3, 5 (1951).
[9] G. R. White (private communication); also tables by R. H. Morgan and H. E. Corrigan, Handbook of Radiology (The Year Book Publishers, Inc., Chicago, 1955).
[10] L. S. Taylor and G. Singer, Radiology **15**, 637 (1930).
[11] G. H. Aston and F. H. Attix, Acta Radiol. **46**, 747 (1956).
[12] W. H. Bragg, Studies in radioactivity, p. 94 (MacMillan and Co., New York, N. Y., 1912).
[13] L. H. Gray, Proc. Roy, Soc. (London) [A] **156**, 578 (1936).
[14] U. Fano, Nucleonics **11**, No. 8, 8 (1953).
[15] H. A. Bethe and J. Ashkin, Experimental nuclear physics, E. Segre, Ed., (John Wiley & Sons, Inc., New York, N. Y., 1953).
[16] C. J. Bakker and E. Segre, Phys. Rev. **81**, 489 (1951).
[17] R. M. Sternheimer, Phys. Rev. **88**, 851 (1952).
[18] L. V. Spencer, Phys. Rev. **98**, 1597 (1955).
[19] H. O. Wyckoff (private communication).